

# Astrophysical calibration of gravitational-wave detectors

M. Pitkin,<sup>1,\*</sup> C. Messenger,<sup>1,†</sup> and L. Wright<sup>1,‡</sup>

<sup>1</sup>*SUPA, School of Physics and Astronomy, University of Glasgow, Glasgow G12 8QQ, United Kingdom*  
(Dated: March 6, 2022)

We investigate a method to assess the validity of gravitational-wave detector calibration through the use of gamma-ray bursts as standard sirens. Such signals, as measured via gravitational-wave observations, provide an estimated luminosity distance that is subject to uncertainties in the calibration of the data. If a host galaxy is identified for a given source then its redshift can be combined with current knowledge of the cosmological parameters yielding the true luminosity distance. This will then allow a direct comparison with the estimated value and can validate the accuracy of the original calibration. We use simulations of individual detectable gravitational-wave signals from binary neutron star (BNS) or neutron star-black hole systems, which we assume to be found in coincidence with short gamma-ray bursts, to estimate any discrepancy in the overall scaling of the calibration for detectors in the Advanced LIGO and Advanced Virgo network. We find that the amplitude scaling of the calibration for the LIGO instruments could on average be confirmed to within  $\sim 10\%$  for a BNS source within 100 Mpc. This result is largely independent of the current detector calibration method and gives an uncertainty that is competitive with that expected in the current calibration procedure. Confirmation of the calibration accuracy to within  $\sim 20\%$  can be found with BNS sources out to  $\sim 500$  Mpc.

PACS numbers: 04.80.Nn, 95.55.Ym

## I. INTRODUCTION

It is expected that the advanced generation of interferometric gravitational-wave (GW) detectors will detect waves emitted from  $O(10s)$  of compact binary coalescences (CBCs) per year [1]. One such class of these cataclysmic events, the inspiral and merger of binary neutron star (BNS) systems will be detected out to a maximum range (horizon distance) of  $\approx 450$  Mpc. Assuming the current best estimates for the cosmological parameters, this is equivalent to a redshift  $z \approx 0.1$ . As noted by Schutz [2], CBC systems can be used as cosmological distance markers, otherwise known as “standard sirens” (analogous to electromagnetic (EM) standard candles). The nature of these sources will allow us to estimate, among other parameters, their luminosity distance without the need for calibration against the cosmic distance ladder.

It is considered likely that the merger of BNS and/or neutron star-black hole (NSBH) systems, in addition to emitting detectable GWs, is also the mechanism for producing short gamma-ray bursts (sGRBs) [3]. In this scenario these events produce tightly beamed EM emission parallel to the orbital angular momentum vector of the system. Additional evidence for the coincidence of sGRBs with GW events is the estimated astrophysical rates of both phenomena. Observations of sGRBs give an inferred rate of sGRB producing CBC mergers of  $8 \times 10^{-9}$ – $1.1 \times 10^{-6}$  Mpc<sup>-3</sup> yr<sup>-1</sup> [4] after accounting

for beaming effects. This can be compared to independently obtained estimates of BNS merger rates of  $10^{-8}$ – $10^{-5}$  Mpc<sup>-3</sup> yr<sup>-1</sup> [1], or NSBH merger rates of  $6 \times 10^{-10}$ – $1 \times 10^{-6}$  Mpc<sup>-3</sup> yr<sup>-1</sup> [1]<sup>1</sup>.

If a single GW event is observed in coincidence with a sGRB it may be possible to identify the host galaxy of the source. With this information a spectroscopic redshift can be very accurately obtained (see values quoted in e.g. [6] and references therein). With knowledge of the redshift, using current best estimates for the Hubble constant and other cosmological parameters, the true luminosity distance can be estimated to  $\sim 1\%$  accuracy [7]. The GW measurement acts as a standard siren also giving us a direct measurement of the luminosity distance to the source. The accuracy of such a measurement depends on a number of factors including the accuracy with which the GW detector has been calibrated. Hence, by comparison with the distance estimate from the sGRB we can recalibrate (or validate) the existing experimentally obtained calibration.

In this paper we investigate the feasibility of this approach for single coincident GW–sGRB events and establish the validation power of such a calibration technique. In Sec. II we briefly summarize the existing experimental technique for GW detector calibration and its expected accuracy. We then review the concept of GW standard sirens and their proposed coincident EM signatures, the sGRBs in Secs. III–IV. In Secs. V–VI we discuss our analysis method and the results, and in Sec. VII we conclude.

\* matthew.pitkin@glasgow.ac.uk

† christopher.messenger@glasgow.ac.uk

‡ Now at: School of Mathematics and Physics, Queen’s University Belfast, Belfast BT7 1NN, United Kingdom

<sup>1</sup> However, the recent work of [5], which studied known galactic BNS systems in more detail, suggests a rate approximately five times lower.

## II. GRAVITATIONAL-WAVE DETECTOR CALIBRATION

The technique used throughout GW research in calibrating the detectors is carried out through a complicated system of physical manipulations of the Fabry-Pérot Michelson interferometer, where an elaborate feedback system is used to sustain a defined measurement in arm length difference between the moving mirrors. A comprehensive description of the calibration procedure (in particular for the LIGO detectors during their fifth science run) can be found in [8], and a brief description is given in [9] and references therein. For Advanced LIGO (aLIGO) and Advanced Virgo (AdV), at the frequency range used in this analysis (20–400 Hz), the error in the strain amplitude calibration is expected to be roughly 10% [9]. This is a benchmark set for the error estimation using the proposed method in this project.

The GW strain is measured through the differential arm length,  $\Delta L$ , changes of the interferometer via  $h(f, t) = \Delta L(f, t)/L$ , where  $L$  is the full arm length. Calibration is required to relate the actual measured interferometer error signal output  $e(f, t)$  to  $\Delta L$ . This relation is known as the length response function,  $R(f)$ , defined such that

$$\Delta L(f, t) = R(f)e(f, t), \quad (1)$$

where we assume  $R$  varies only slowly in time (in comparison to transient signal time scales). Calculation of  $R$  requires the measurement of various functions within a control feedback loop (see [8]), each of which are subject to measurement uncertainties. In this study we assume an estimate of  $R$  is available (although in theory we could take on the role of estimating  $R$  itself), but that it differs from the truth through some unknown scale factor,  $\mathcal{C}$ , so that at a particular time we have

$$\mathcal{C}h(f) = h_m(f) = \frac{R(f)e(f)}{L}, \quad (2)$$

where  $h(f)$  is the true strain and  $h_m(f)$  is the measured strain (i.e. the measured length response function  $R(f)$  is related to the true length response function  $R_{\text{true}}(f)$  via  $R(f) = \mathcal{C}R_{\text{true}}(f)$ ). With this definition it means that if  $\mathcal{C} > 1$  then a signal would appear to have a larger amplitude (i.e. for a given system, would seem closer) than in reality<sup>2</sup>, whereas if  $\mathcal{C} < 1$  it would appear to have a lower amplitude than reality. In this analysis we simplify the situation by assuming that  $\mathcal{C}$  is a constant with respect to frequency (and is real, so has no phase component), but in future studies that assumption could be dropped and  $\mathcal{C}$  could take some functional form, or piecewise fit, with respect to  $f$  [e.g. in a similar way to the method of [10] used for fitting differences in power spectral density (PSD) estimates].

<sup>2</sup> However, the signal-to-noise ratio (SNR) would be the correct value as the signal and the noise will both contain the same scale factor.

## III. BINARY NEUTRON STAR STANDARD SIRENS

The idea of GW standard sirens is directly analogous to the concept of standard candles in EM astronomy and was first proposed in [2]. Unlike the primary EM standard candle event, type Ia supernovae, the measured luminosity of a CBC in GWs is not only a function of distance. It also depends upon the chirp mass (a function of the component masses) and the binary orientation with respect to the global network of GW detectors. However, measurement of the phase evolution of such an event allows accurate determination of the chirp mass<sup>3</sup>. Timing information from the different signal arrival times at each detector in the network allows some level of sky position determination [11]. Finally, amplitude variation between differently oriented interferometers allows some (weaker) level of determination of the binary system orientation.

Standard sirens are clearly a very powerful tool for GW cosmology since they give us a direct measure of the absolute luminosity distance to sources. This is distinct from type Ia supernovae standard candles that only provide relative luminosity distance measures and require calibration via other methods as part of the cosmological distance ladder. The use of GW events with sGRB counterparts for use as a cosmological tool was investigated in [12]–[13] with respect to the third generation GW interferometer, the Einstein Telescope [14] and in [15] for the Advanced detector network. In this case, the redshift information obtained from the sGRB host galaxy provides a complementary measurement allowing each event to inform the distance-redshift relationship and hence obtain cosmological parameter estimates. Other methods for cosmological inference (see [15–19]) have been proposed for BNS systems that do not rely on any redshift measurements. These instead use either the distribution of measured SNRs and assumed form of neutron star (NS) mass and spatial distributions or exploit the features of the tidal and postmerger hypermassive NS stages of the GW waveform.

To put the existing work on GW cosmology in context with the study described in this manuscript we are essentially turning the standard cosmological problem upside down. We assume that the existing EM cosmological parameter estimation [specifically for the Hubble constant, which has uncertainties of  $O(1\%)$  [7]] is accurately determined and therefore a known quantity. We then assume that the unknown in our analysis is the absolute amplitude calibration of the interferometers in the global GW detector network.

<sup>3</sup> In reality it is the redshifted chirp mass that is measured.

#### IV. GRB COUNTERPARTS

It is believed that sGRBs (those gamma-ray bursts with duration  $< 2$  sec) are emitted during the merger of BNS or NSBH systems [3, 20]. The emission from these events is highly beamed along the binary rotation axis and hence only potentially observable for a fraction of the mergers. If the event exhibits an optical afterglow then the host galaxy can be identified, from which a redshift can be obtained (e.g. [21]). The fraction of events with associated redshifts is  $\sim 1/3$ <sup>4</sup>. The range to which the *Swift* x-ray telescope has detected sGRBs is  $z \sim 2$  and the nearest event with associated redshift is at  $z \sim 0.1$  [22], which is approximately equal to the horizon range of the advanced GW detector network for BNS systems.

The predicted detection rates of BNS events (irrespective of an sGRB counterpart) are derived from three main sources: population synthesis models, extrapolations based on known galactic BNS systems, and observations of sGRB events. Various studies using the first two methods have been compiled into an overall detection rate of 0.2–200 BNS events per year [1, 23]<sup>5</sup>. A similar event rate of 1–180 was obtained in [4], where the rate of observed sGRBs was converted to the rate of BNS events by assuming a beaming angle of  $15^\circ$ . The beaming angle is the primary factor in determining the fraction of detected GW BNS signals with an EM sGRB counterpart and is unfortunately highly uncertain. Various authors have provided estimates on the rate of joint detections to be in the range 0.02–7 per year [24–27].

The most likely scenario in which a coincident GW–sGRB event would be identified is through the targeted follow-up of an observed GW or by *post facto* matching of GW trigger lists with known (or subsequently found [28]) sGRB events. The likelihood of being able to follow-up GW events using gamma-ray telescopes with low enough latency to catch a sGRB is low. Compounding this issue is the relatively large GW sky error box giving a field of view for the EM observatories to search spanning  $\sim 100$ s of square degrees (e.g. [11, 23, 29]). For the scenario of a GW-followup of an observed sGRB, the merger time for BNS/NSBH systems will be estimated from the sGRB to within a few seconds (see e.g. the discussion in Sec. 2.2 of [30]). This makes the follow-up search less computationally expensive since it is performed over a smaller range of data using potentially fewer numbers of waveform templates. This computational saving enables the use of

a more computationally expensive multi-detector coherent scheme rather than the cheaper coincidence methods used in the untargeted searches.

A fortunate consequence of a joint GW–sGRB observation will be the fact that in order for such an event to be observed, the BNS/NSBH system must have had its orbital angular momentum vector pointing towards (or away) from the detector. The actual inclination angle of the system, defined as the angle between the orbital angular momentum vector and the line of sight, must be  $<$  half of the sGRB beaming angle. This prerequisite property limits us to systems that are approximately “face-on” and therefore effectively optimally oriented. At given distances this makes us biased towards higher SNR signals but it is more meaningful to think of this as an increase in the sensitivity range of the detectors. However, as discussed earlier, the property of beaming severely impacts the probable rate of such joint observations.

#### V. ANALYSIS

The main aim of this work is to assess how well the calibration scale factor defined in Eq. 2 can be estimated from a single observed GW associated with a particular sGRB. As we *a priori* have little knowledge of the likely location and distance of such an event we have performed simulations of multiple events to see the distribution in the accuracy of the calibration scale factor recovery.

For all our signals we use the TaylorF2 waveform approximation (see e.g. [31] and references therein) with a 3.5 post-Newtonian expansion in phase for modeling our signal (in both simulations and signal recovery). For BNS systems we use nonspinning waveforms under the assumption that the component spins will be small and have a negligible effect on the analysis<sup>6</sup> (see discussion in [11] and studies in [32]). For NSBH systems we use a spinning waveform, but in which only the black hole has non-negligible spin and its rotational angular momentum is aligned with the system’s orbital angular momentum.

For a nonspinning system the general form of the frequency-domain polarization amplitudes is

$$\begin{aligned}\tilde{h}_+(f) &\propto (1 + \cos^2 \iota) D_L^{-1} \mathcal{M}^{5/6} f^{-7/6} e^{-i\Psi(f, \mathcal{M}, t_c, \phi_c)}, \\ \tilde{h}_\times(f) &\propto \cos \iota D_L^{-1} \mathcal{M}^{5/6} f^{-7/6} e^{-i\Psi(f, \mathcal{M}, t_c, \phi_c)}\end{aligned}\quad (3)$$

where the chirp mass  $\mathcal{M}$  is defined as  $\mathcal{M} = M q^{3/5}$ , with the symmetric mass ratio  $q = m_1 m_2 / M^2$ , total mass  $M = m_1 + m_2$  (where  $m_1$  and  $m_2$  are the component masses), and  $\iota$  is the binary inclination angle. The Fourier transform of the GW strain measured at the  $k^{\text{th}}$  detector is then given by

$$\tilde{h}^k(f) = F_+^k(\alpha, \delta, \psi) \tilde{h}_+(f) + F_\times^k(\alpha, \delta, \psi) \tilde{h}_\times(f) \quad (4)$$

<sup>4</sup> [http://swift.gsfc.nasa.gov/archive/grb\\_table/](http://swift.gsfc.nasa.gov/archive/grb_table/)

<sup>5</sup> We note that this rate is that given in Table I of [23] for an aLIGO and AdV network consisting to two aLIGO detectors operating at design sensitivity. However, a higher rate of 0.4–400 is given in [1], which may differ due to the use of a third aLIGO detector, but the discrepancy may also have contributions from slightly different threshold definitions or design sensitivity curves used. We also note the study mentioned in Sec. I that potentially lowers the expected rate by a factor of five.

<sup>6</sup> In future studies we could create our simulations including small spins and confirm that this does not have a significant effect on our results if recovery is with nonspinning templates.

where  $F_+^k$  and  $F_\times^k$  are the antenna response functions which are dependent upon the polarization angle  $\psi$  and the sky position of the source with right ascension  $\alpha$  and declination  $\delta$ .

For this analysis we consider the advanced generation aLIGO and AdV detectors operating at their design sensitivity, with noise power spectral densities taken from [23]. The detector network we consider consists of the two aLIGO detectors (H1 and L1) and the AdV detector (V1).

We consider that the measured data in any detector are defined as

$$\tilde{d}_k(f) = \mathcal{C}_k(\tilde{n}_k(f) + \tilde{h}_k(f, \boldsymbol{\theta})) \quad (5)$$

where  $\tilde{n}(f)$  is the Fourier transform of the true (in this case Gaussian) strain noise,  $\boldsymbol{\theta}$  is the set of waveform pa-

rameters and  $\mathcal{C}_k$  is the calibration scale factor for the  $k^{\text{th}}$  detector, which are the parameters we are interested in estimating.

## A. Method

To assess the ability to estimate the unknown calibration scale factors we calculate their marginal posterior probability distribution functions (PDFs). We use Bayes' theorem for which we need to define a likelihood function and prior PDFs on the signal parameters and the calibration scale factors. In this analysis we use the Markov chain Monte Carlo (MCMC) code `emcee` [33] to sample the posterior distribution. We use a Gaussian likelihood function given by

$$p(\mathbf{d}|\boldsymbol{\theta}, \mathcal{C}, I) \propto \exp \left[ 4\Delta f \sum_{k=1}^{N_{\text{det}}} \sum_{i=i_{\text{low}}}^{i_{\text{high}}} \frac{\Re \left\{ \tilde{d}_{k,i}^* \mathcal{C}_k \tilde{h}_{k,i}(\boldsymbol{\theta}) - \frac{1}{2} \left( \mathcal{C}_k^2 \tilde{h}_{k,i}^*(\boldsymbol{\theta}) \tilde{h}_{k,i}(\boldsymbol{\theta}) + \tilde{d}_{k,i}^* \tilde{d}_{k,i} \right) \right\}}{S_{k,i}} \right] \quad (6)$$

where  $\mathbf{d}$  is an array containing the data for all detectors,  $\Delta f$  is the frequency resolution,  $S_k$  is the  $k^{\text{th}}$  detector's estimated one-sided noise PSD (and as such will contain the effect of the calibration scale factor), and the  $i$  indices increment over frequency with  $i_{\text{low}}$  and  $i_{\text{high}}$  corresponding to the lower and upper range in frequencies used for our analysis, which were 20 to 400 Hz respectively. This frequency range was chosen as the vast majority of the SNR for the inspiralling signals we use can be found within it (for a typical BNS system of two  $1.4 M_\odot$  stars, or a NSBH system with component masses of  $5 M_\odot$  and  $1.4 M_\odot$ , only  $\sim 3 - 4\%$  more SNR is gained by using a 10 to 1500 Hz frequency range), so going to lower or higher frequencies provides very little additional information while increasing the computational cost<sup>7</sup>. The source parameters have been subsumed into a vector  $\boldsymbol{\theta}$  and the calibration scale factors are within the vector  $\mathcal{C}$ .

### 1. Prior ranges

The primary reason why coincident observations with a sGRB can be used as a check of detector calibration is that the sGRB allows us to constrain the priors on various parameters that would normally be highly correlated with the signal amplitude. The most important of these

is that the sGRB can provide a very tight constraint on the source distance. In this analysis we therefore assume that the source distance is known (i.e. has a  $\delta$ -function prior) whereas in reality the error on this distance will be dependent upon the uncertainties in both the redshift measurement and the Hubble constant. For spectroscopic redshifts this uncertainty will be dominated by the Hubble constant and will be of  $O(1\%)$ .

Other information relevant for a coincident sGRB is that the system is likely to be relatively close to face on (and therefore nearly circularly polarized), which allows us to place prior constraints on the system inclination angle. Beam opening angles for sGRBs are relatively poorly constrained as they are based on only a few jet-break detections. A comparative study of estimates and lower limits of opening angles for 13 sGRBs given in [34] provides a median opening angle value of  $\sim 10^\circ$ . We use this median opening angle as a rather conservative guide to form a Gaussian prior distribution on the system inclination angle,  $\iota$ , by converting it into an equivalent standard deviation for a half-normal distribution. We therefore place a Gaussian prior on  $\iota$  with zero mean and a standard deviation  $\sigma = 14.8^\circ$ . This, and the choice of polarization angle prior range given below, explicitly fixes the handedness of the system's rotation (or alternatively whether it is face on or back on). If we were to allow the inclination to have two modes (one for face on and one for back on), or alternatively to double the range of the polarization angle, it would have no effect on our ability to estimate the signal amplitude as the two modes should be identical with regards to the amplitude parameter probability distributions. However, we are consistent between the range of simulated signals dis-

<sup>7</sup> In a real analysis, rather than this case study, the additional computational cost of using a larger frequency range may be worthwhile, but in this case we had to run many simulations and the computational cost was a limiting factor.

cussed in Sec. VB and the initial ranges stated.

The prior on the system component masses is dependent on whether we are considering the source being a BNS system or a NSBH. For the former case the prior we use is a Gaussian distribution for both components with means of  $1.35 M_\odot$  and standard deviations of  $0.13 M_\odot$ , which is roughly consistent with the double neutron star system masses found in [35] albeit with a wider distribution. In reality, for all the systems we use in our study, the chirp mass, which we see from Eq. 3 plays a role in the overall signal amplitude, is very well constrained by the system's phase evolution, so our prior could be expanded with minimal effect on the results. In the case of NSBH systems we use the same prior as above for the neutron star, but for the black hole we use a prior based on the canonical mass distribution used for the rate results in [36] with a mean of  $5 M_\odot$  and a standard deviation of  $1 M_\odot$ . We note that the mass range of black holes could be quite different from this, but use this range as an example for this type of system. For the NSBH systems we also require a prior on the black hole spin (for BNS systems we have assumed that the spins are small enough that they will be negligible). We use a uniform prior on the normalized aligned spin magnitude between  $-1$  and  $1$ .

The final important piece of information that we can make use of from the sGRB observation is the sky position of the source. We assume that this is known precisely and has been obtained, in conjunction with the source redshift, from the identification of the host galaxy. This fixes the time delay between detectors to a known value and, along with the polarization angle, defines the antenna response patterns.

For the time of coalescence  $t_c$  we use a uniform prior spanning  $\pm 0.01$  seconds around the recorded time of the signal that would be returned by the GW detection pipeline. For the reference phase  $\phi_c$  a uniform prior on the range  $(0, \pi]$  is used, and for the polarization angle we use a uniform prior on the range  $(0, \pi/2]$ . As the signals we use are generally close to being circularly polarized (face on) the phase and polarization angle will be largely degenerate and their exact combination will have little effect on the result.

Finally, we require a prior on the calibration scale factors for each detector. We make the assumption that in general the calibration applied to the detector data will be close to being correct, so we want to use a prior that is peaked at  $C_k = 1$ . We also (naïvely) assume that the prior PDF of the calibration scale factor is either larger or smaller than unity by an equivalent factor, e.g.  $p(C = 10|I)$  is equivalent to  $p(C = 0.1|I)$ . For the scale factor in each detector we therefore use the following log-normal distribution as our prior,

$$p(C|I) = \frac{1}{C\sigma\sqrt{2\pi}} \exp\left(-\frac{(\ln C - \mu)^2}{2\sigma^2}\right), \quad (7)$$

where we chose  $\sigma = 1.07$ , which together with the requirement that the mode is at unity gives  $\mu = 1.15$ .

With these parameters the prior probability density at  $0.1$  and  $10$  is one tenth of that at  $1$  making this a fairly conservative prior designed to have little impact on our results. Note that this prior does not give a symmetric amount of probability about unity (so our prior favors  $C$  values greater than  $1$ ), but given our simulation criterion described in Sec. VB we find that the likelihood generally overwhelms the prior and our naïve assumptions have little effect.

## B. Simulations

To estimate how well the calibration scaling can be constrained for each detector in an advanced detector network we have performed analyses with simulated BNS and NSBH signals. These were simulated at a range of distances:  $50$  to  $500$  Mpc with  $50$  Mpc increments for the BNS signals and  $100$  to  $900$  Mpc with  $100$  Mpc increments for the NSBH signals. The simulations used the two aLIGO detectors (H1 and L1) and the AdV detector (V1) and were all performed in the frequency domain and spanned a frequency range from  $20$  to  $400$  Hz, which is a range that contains the vast majority of the SNR and is therefore all that is required to provide good constraints on  $C$ . We assumed all detectors were operating at their design sensitivity (as given by Fig. 1 of [23]). As such we added colored Gaussian noise to each simulation based on the sensitivity curve, but scaled with the associated calibration scale factor.

Separately for the BNS and NSBH systems we have performed a large number [several hundred up to  $O(1000)$ ] of simulations at each distance value. When proposing injections for each simulation the source parameters were randomly drawn from the prior distributions described in Sec. VA 1, with the sky position being drawn randomly from a uniform distribution on the sky, the coalescence times held fixed within the center of the prior window, and with the calibration scaling factors for each detector drawn from a Gaussian distribution with a mean of one and standard deviation of  $0.125$  (equivalent to a mean fractional offset of  $10\%$ ). Note that this distribution is broadly consistent with the scale of calibration uncertainties that is expected via experimental methods, but is not the same as the prior that we assume on  $C$  [see Eq. 7] when recovering signals<sup>8</sup>.

In accepting a proposed simulation as one to be analyzed we introduced a criterion that the signal be “detectable”, based on that used in [36]. We therefore only analyzed simulations that had an SNR of  $\geq 5.5$  in at

<sup>8</sup> The reason behind this is that we wanted to use a fairly naïve and conservative prior for signal recovery that had little impact in the results, i.e. to produce results dominated by the likelihood for these parameters. However, limited studies using  $C$  values within the much larger range of  $\sim 0.1$  to  $10$  show distributions with consistent relative widths to those we find in our main study.

least two detectors. Since we assume that these signals would be coincident with a sGRB we do not include the often used further constraint that the total coherent network SNR is greater than 12. For simulations close to the SNR threshold, the application of the threshold resulted in the preferential selection of better oriented systems. Therefore, at larger distances the population of injected sources was not uniformly distributed over the sky and instead favored locations with better antenna response. Similarly, despite already being constrained by the prior to small inclination angles, the accepted simulations show preference for sources very close to circularly polarized.

These simulations have allowed us to assess how well on average we would be able to constrain the calibration scale for a detected CBC-sGRB coincidence.

## VI. RESULTS

A simple assumption that one could make would be that the uncertainties on the calibration scale factors (if they are independent of other parameters and have a roughly Gaussian probability distribution) should be given by  $\sim 1/\text{SNR}$  for each detector. As we show below this assumption is reasonable, but small correlations do exist between parameters meaning that it does not completely hold.

For each of the simulated sources we have used the `emcee` python MCMC package [33] to perform parameter estimation over the unknown source parameters using the priors as discussed in Sec. V A 1. In each case when calculating the likelihood we used an estimate of the noise PSD based on the advanced detector design sensitivities (using those given in [23]), but calculated by averaging 64 separate noisy realizations of the PSD and scaled with the same calibration scale factor as applied to the injection and noise<sup>9</sup>. This has provided posterior probability distributions<sup>10</sup> on the calibration scale factors for each detector. Examples of the marginalized posterior probabilities for a BNS system and a NSBH system observed with the three detector network are shown in Figs. 1 and 2 respectively.

From these posterior distributions we have calculated the minimal 68% credible region for the calibration scale factors for each detector (if these were Gaussian distributions this is equivalent to the region either side of the

mean bounded by the  $1\sigma$  intervals). For all the signals at each distance increment we have produced the distribution of the fractional half widths (i.e.  $1\sigma$ ) of these scale factors' confidence intervals compared to the true value. These are shown as boxplots in Figs. 3 and 4 for the BNS and NSBH systems respectively. The boxes show the extent from the lower to upper quartile of the values, while the whiskers extend from the fifth to 95<sup>th</sup> percentile. The black line within each box gives the median value and the star gives the mean value. Also shown on each plot as the dashed magenta line is the percentage of signals drawn from the prior distribution that fulfils the detection criterion.

In Fig. 3 we see that on average the scale factor can be recovered to equivalent precision in both aLIGO detectors, as would be expected, with uncertainties generally within the 10% range for sources at 100 Mpc. This is comparable to previous estimates of the calibration error in the initial LIGO detectors. An interesting feature is that for distances  $\gtrsim 250$  Mpc the upper extent of the uncertainty for H1 and L1 hits a maximum at  $\sim 25\%$ , while the width of boxes narrows. This is due to our “detectability” criteria, where for all distances we only see those sources with a high enough SNR that we would consider them detectable, i.e. the weakest signals that could still be detected would always have a single detector SNR of  $\sim 5.5$  no matter their distance, hence the plateau. In addition there will also be fewer sources with SNR higher than this criteria at large distances, giving us a narrower range, and we automatically exclude those with SNR that are too small thus truncating our uncertainty distribution at the upper end. However, this does show that on average for sources that are detectable out to 450 Mpc we would be able to constrain the calibration scale factor uncertainty for the aLIGO detectors to  $\sim 20\%$ .

The largest SNR contribution will generally come from the two aLIGO detectors and thus the detection criteria (SNR threshold) will not apply to the AdV result. Hence, the SNR in AdV can be small and thus the ability to constrain its scale factor becomes poor (although it still provides information that the calibration is not grossly inaccurate). We also see that true uncertainties achievable for recovering the calibration scale factors are indeed very similar to the simple assumption that they would be given by  $\sim 1/\text{SNR}$ , i.e. at the upper end of the distribution the SNR in the two aLIGO detectors will be  $\sim 5.5$ , which would be expected to produce uncertainties of  $\lesssim 20\%$ . Our results are slightly poorer than estimates based on this simple assumption due to correlations with  $\iota$  even within the constrained prior range, and slight correlations between the scale factors for H1 and L1 as seen in Fig. 1.

In Fig. 4 we see very similar results for the NSBH systems although the higher SNR of the signals means that we can provide  $\sim 20\%$ – $25\%$  uncertainties on the calibration scale factors for H1 and L1 out to greater distances. The distributions generally appear slightly broader than

<sup>9</sup> We do not account for there being a potential difference between the estimated PSD and the actual PSD of the analysed section of data as described in e.g. [10]. This difference would be very highly correlated with the calibration scale factor, so in reality our estimate of the scale factor would be a combination of the calibration offset and the difference in the PSD. As such our results on real data would be an upper limit on the calibration scale factor.

<sup>10</sup> As a proxy to check for convergence of the MCMC chains we check that the calibration scale factor posterior histograms do not contain many disjoint modes.

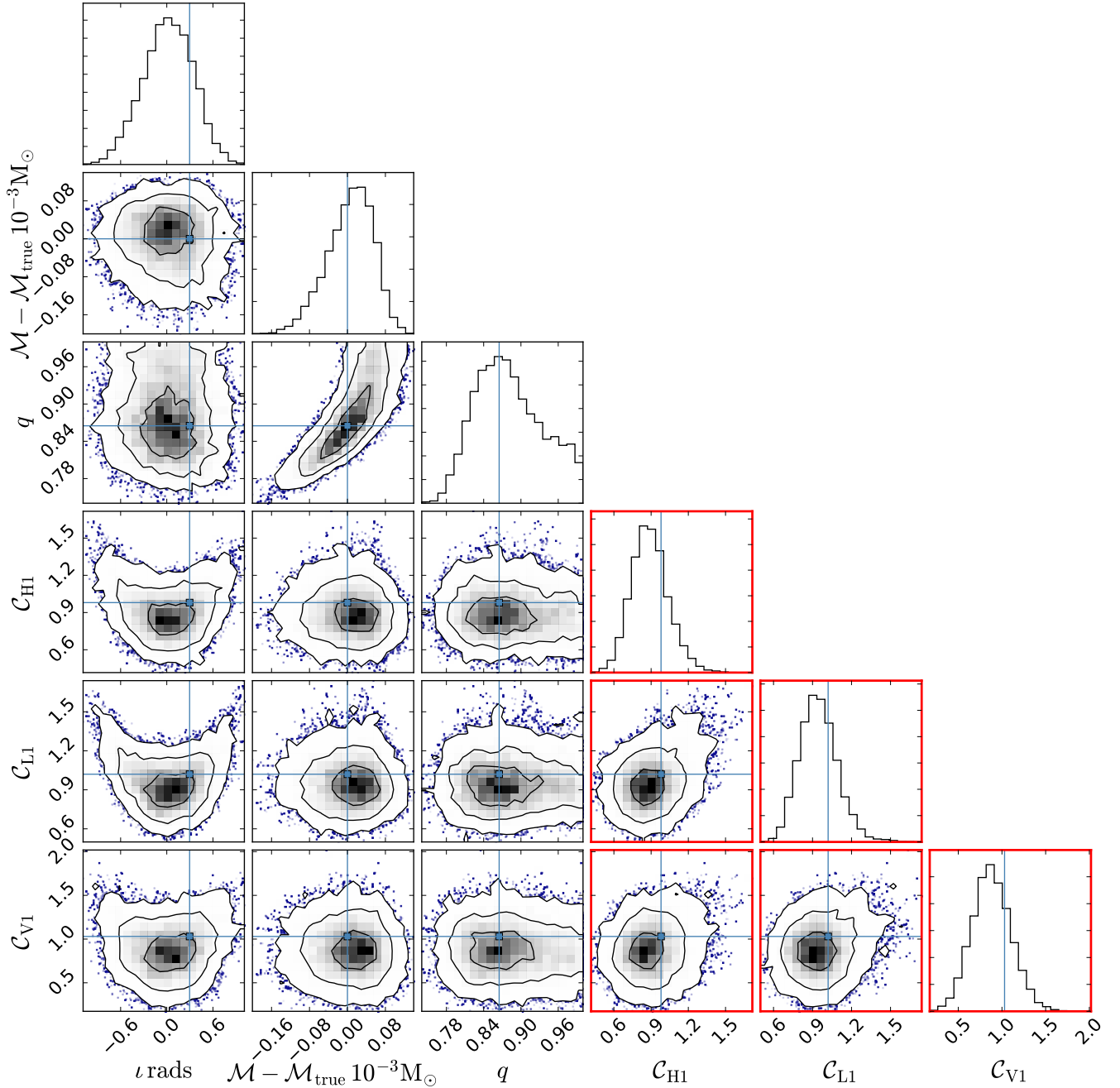


FIG. 1: The marginalized posterior probability distributions for some of the unknown parameters of a BNS system, including calibration scaling factors (surrounded by the thicker red borders) for the three detectors (H1, L1 and V1). The simulated signal was at a distance of 250 Mpc, had SNR of 7.9, 9.1 and 5.2 and percentage relative uncertainties in the calibration scale factors of 15%, 14% and 22% for each of the detectors respectively.

those for the BNS systems. This may be explained by two factors. The first is from the fact that including the spin parameter leads to strong correlations between the chirp mass, mass ratio and spin. These strong correlations make convergence of the MCMC take longer and means we have fewer independent samples with which

to estimate the posterior distributions. This leads to a larger statistical fluctuation on the results. The second factor is that there appears to be a modest effect due to the population of sources that is detectable. For distances at which the BNS and NSBH systems would give the same percentage of observable sources there is a slight

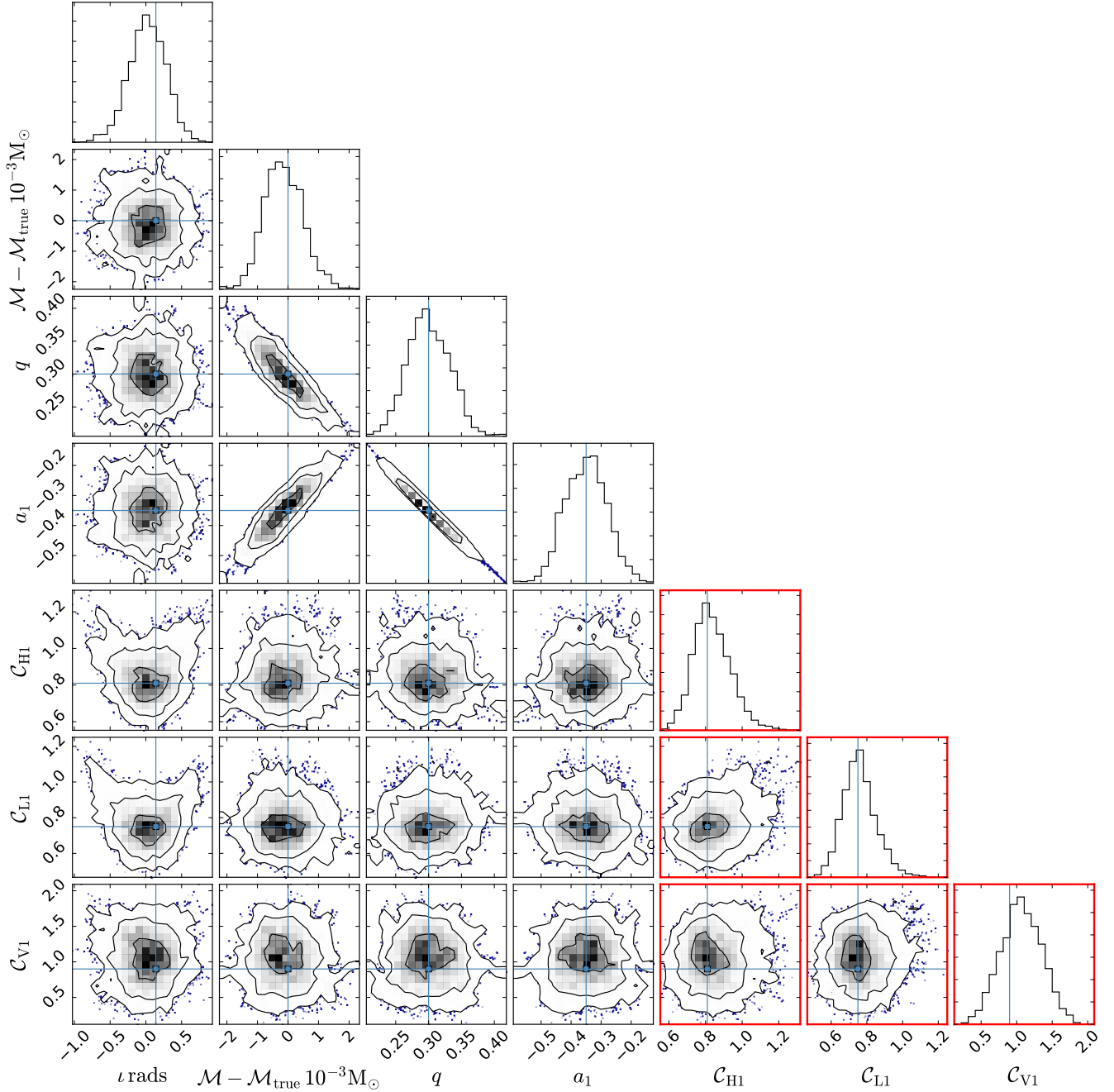


FIG. 2: The marginalized posterior probability distributions for some of the unknown parameters of a NSBH system, including calibration scaling factors for the three detectors (H1, L1 and V1). The simulated signal was at a distance of 450 Mpc, had SNR of 9.7, 10.3 and 3.8 and percentage relative uncertainties in the calibration scale factors of 14%, 13% and 43% for each of the detectors respectively.

increase in the mean and standard deviation of SNRs of the NSBH systems over the BNS systems.

As noted previously, the mass distribution for black holes could be quite different from the one used here, with masses extending to  $\gtrsim 10 M_{\odot}$ . We expect these would produce similar results to those we see in Fig. 4, but

again extending to further distances. However, at higher masses we would encounter the problem that the chirp mass will be less well constrained due to there being fewer observable cycles during the inspiral stage. Including the merger and ring-down phase, which we currently ignore, will also increase SNR and act to reduce the calibration



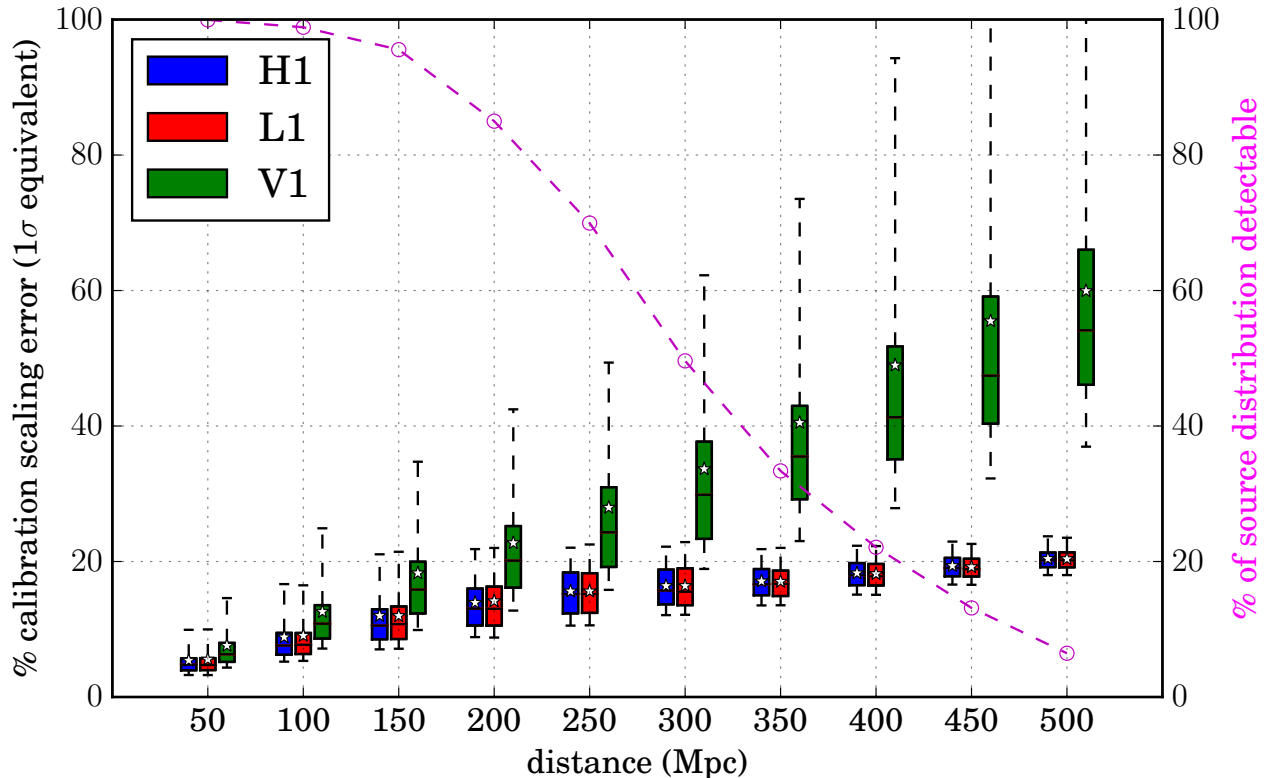


FIG. 3: Distributions of the percentage accuracy at which the calibration scale factors can be determined for a three detector network using BNS systems (provided a coincident GRB is observed and can yield a distance estimate). The boxplots span the lower to upper quartile range of the distributions, with the median value shown as a horizontal line within the box and the mean shown as a white star. The dashed magenta line shows the percentage of sources drawn from the prior distribution that would be detectable at each distance value.

scale uncertainties, provided there is sufficient SNR in the inspiral to constrain the chirp mass.

#### A. Parameter biases

It is also interesting to see if our analysis has any bias on the recovered  $\mathcal{C}$  PDFs, or whether they are recovered in a way that is consistent with the simulated values. To do this we have produced plots showing the cumulative fraction of the true (simulated)  $\mathcal{C}$  values recovered within given posterior credible intervals (see e.g. [37] for the initial use of this type of plot to check consistency of GW analyses) for the BNS systems at 50 and 500 Mpc (see Fig. 5). Self-consistent PDFs should show that a fraction of injected values falls within the corresponding credible interval, and therefore the cumulative fraction should lie along the diagonal of the plot. Any biases would show up as significant deviations from the diagonal.

Figure 5a shows that for sources at 50 Mpc there is no highly significant bias on the recovery of  $\mathcal{C}$  for any of the detectors. However, in Fig. 5b, with sources at

500 Mpc, while H1 and L1 follow the diagonal well, V1 goes significantly above the diagonal. This shows that the PDFs on  $\mathcal{C}$  for V1 are too broad. The reason for this is that at these larger distances the PDFs on  $\mathcal{C}$  for V1 are not well constrained and start to become dominated by the prior. As we have previously noted this prior is not the same as the distribution used to generate the  $\mathcal{C}$  values, but is instead far broader and more conservative. So this bias is showing up due to the simulated values of  $\mathcal{C}$  being generated from a much more narrow range.

Despite the inconsistency in V1 it is satisfying to see that for the detectors for which the  $\mathcal{C}$  values are reasonably constrained (i.e. H1 and L1 in Fig. 3) the actual value is recovered consistently, with little effect from the prior.

## VII. DISCUSSION

We have established how well we can assess the detector calibration for aLIGO and AdV using astrophysical sources as standard sirens. To do this we require that

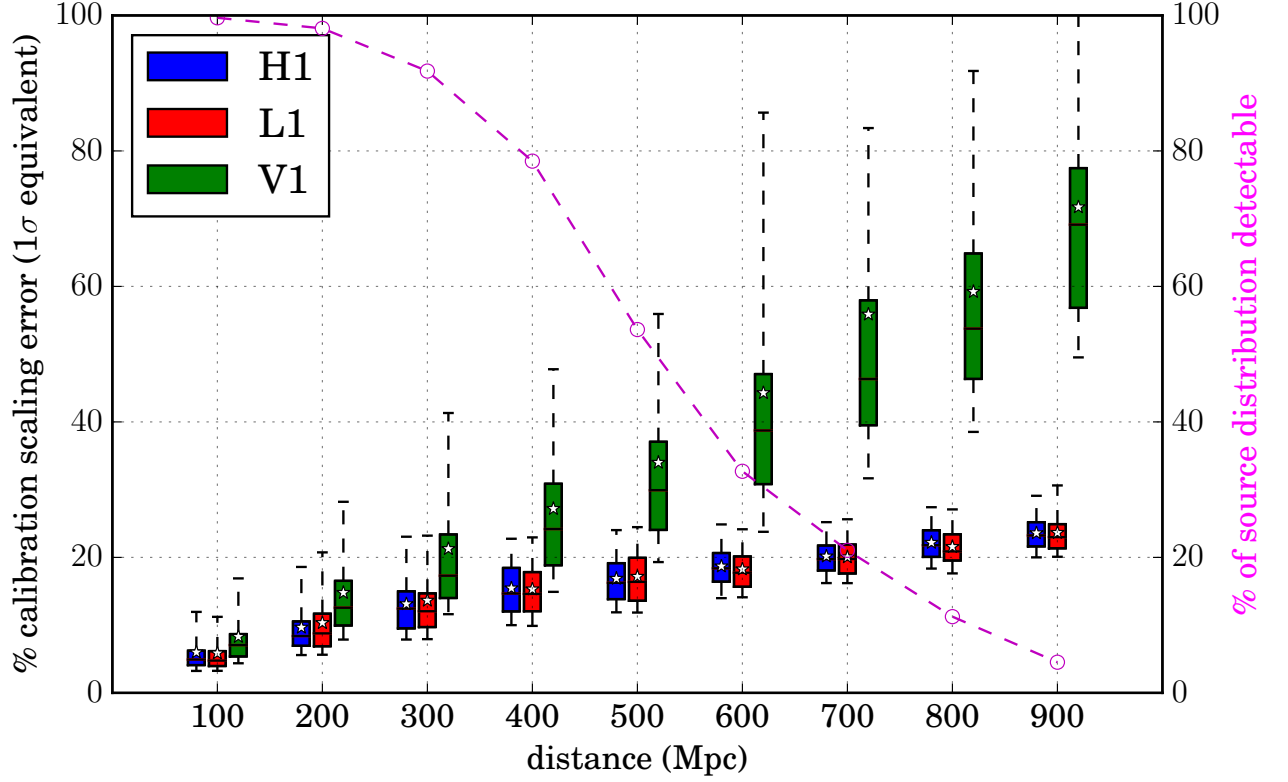


FIG. 4: Distributions of the percentage accuracy at which the calibration scale factors can be determined for a three detector network if using NSBH systems (provided a coincident GRB is observed and can yield a distance estimate). The plot contents are the same as in Fig. 3.

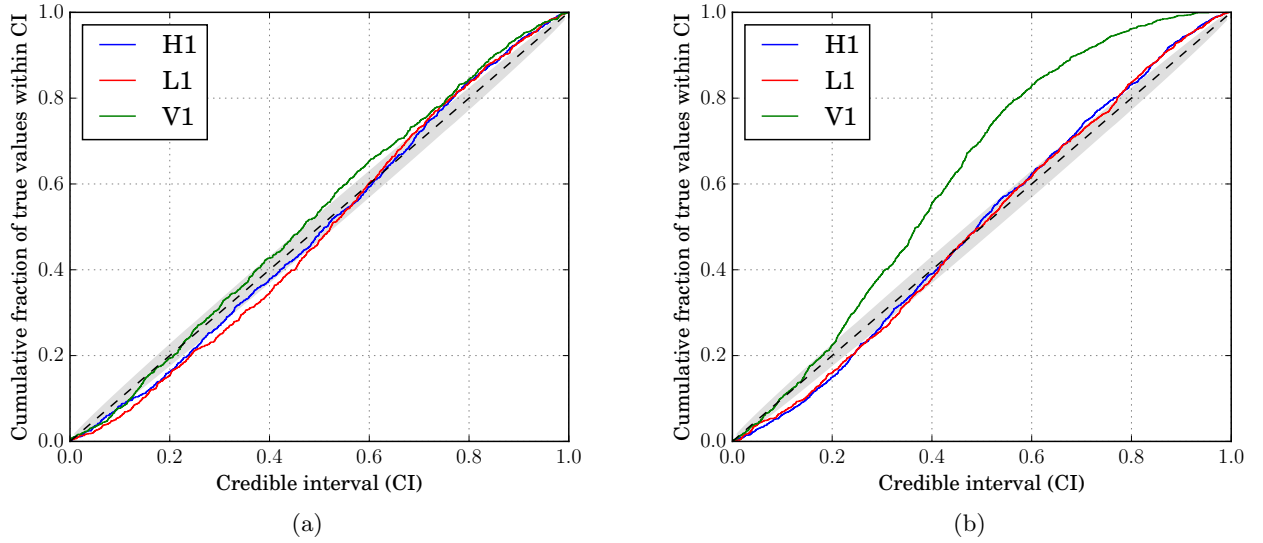


FIG. 5: Both figures show the cumulative fraction of true  $\mathcal{C}$  values found within a given fractional credible interval versus the fractional credible interval for each detector for the BNS simulations at (a) 50 Mpc and (b) 500 Mpc. The grey shaded region is a 95% credible band for the expected deviations from diagonal.

a sGRB, for which it has been possible to measure the distance, is observed in coincidence with a CBC signal in the GW detectors. This enables us to assume a known distance and sky position for the source, and also limit the inclination of the source, which in turn allows us to test the consistency of the detector calibration. We do this by including an unknown scale factor on the true signal and noise, which we estimate given the data from the three interferometer advanced detector network. We find that for detectable BNS sources the uncertainty on the calibration scale factor could on average be determined to  $\lesssim 10\%$  of its true value for the aLIGO and AdV detectors out to 100 Mpc. This is comparable to the proposed accuracy level of the hardware calibration of the detectors. For sources at the standard single detector BNS horizon distance of  $\sim 450$  Mpc the scale factor could on average be determined to within  $\lesssim 20\%$  of its true value for the aLIGO detectors. Similar results were found for NSBH sources, although sources could be observed out to higher distances.

The requirement of a coincident sGRB with a known distance means that there will likely be considerable delay (beyond initial GW detection) for the implementation of this method of calibration assessment. Importantly however, this method would provide an independent<sup>11</sup> consistency check that the calibration is reasonably accurate in addition to the existing calibration methods [8]. We acknowledge that we have made a number of simplifying assumptions, including that the waveforms we use accurately model the true signal, and that the overall calibration remains constant over the duration of a signal and its PSD estimation. A further major simplification made here is that the absolute calibration is constant with frequency. Other authors (e.g. [9, 10]) have addressed this issue in the context of robust parameter estimation for astrophysical sources and in future work we intend to apply related methods for astrophysical calibration. We have also neglected any phase uncertainty in the calibration.

A further application of astrophysical calibration is the relative calibration of GW detectors. In this case we are interested in obtaining posterior distributions on the ratios of calibration scale factors and phases between detectors. For CBC events, in this scenario there would be no explicit requirement for a redshift measurement and therefore a cosmologically inferred distance. There would however be a requirement for an electromagnetically inferred sky position of  $O(\text{degrees})$  accuracy. A more suitable source for relative calibration estimation would be that of continuous GW emission. In that case, sky position and orientation information would be obtained to a high level of accuracy from single detector analyses alone. A primary use for relative calibration information would

be to account for potential biases in the sky position estimates for CBC and burst sources (Vitale, Messenger & Pitkin, in preparation). In this case, amplitude information is a secondary, but important, factor in breaking degeneracies on sky position estimates.

We emphasize that our work has assumed that the PSD used in the likelihood function is an accurate representation of the PSD at the time of the observed CBC signal. In reality the PSD may be estimated from a period close to, but not overlapping, the signal time and therefore may be slightly different [10]. Our result would therefore be highly correlated with any uncertainty in the PSD estimate, but would still offer an upper limit on the calibration uncertainty.

A further extension of this work would be for the calibration scale factor to be estimated as a function of frequency. This may require the frequency series to be divided into sections and the calibration scale factor estimated for each. However, since the scale factor uncertainty is related to the SNR then the SNR contribution in each frequency section is of relevance. In this case Bayesian model selection may be applicable for selecting the optimal number of frequency sections with which to estimate the scale factor. The BayesLine algorithm [38], or the method described in [10], may provide a natural way to perform such an analysis. Indeed these methods, and those of [9] are already being used to marginalize over calibration uncertainties, but do not yet attempt to estimate them.

It is also worth noting that astrophysical calibration may be possible for future planned space-based detectors such as eLISA [39]. For such detectors there are several galactic binary systems known as “verification” binaries [40], in that their masses and orbital parameters allow them to be guaranteed sources. These too could be used for assessing detector calibration. However, generally for these verification binaries the inclination of the system is not known and distances are fairly uncertain, so a precise calibration assessment may not be possible. However, there is at least one currently known eclipsing white dwarf binary (J0651) [41], which does provide the system inclination [42, 43] and has an approximately 10% distance uncertainty [41], which makes it an excellent candidate for an astrophysical calibrator.

## ACKNOWLEDGMENTS

We acknowledge useful discussions within the LIGO-Virgo Collaboration and specifically with Salvatore Vitale. L.W. was part funded for this work through a Royal Astronomical Society Undergraduate Research Bursary. M.P. and C.M. are funded by the Science and Technology Facilities Council (STFC) under Grant No. ST/L000946/1. C.M. is also supported by a Glasgow University Lord Kelvin Adam Smith fellowship. We are grateful for computational resources provided by Cardiff University, and funded by STFC Grant No.

<sup>11</sup> There are caveats to this independence. We rely on a source having been detected, which most likely implies that calibration is not grossly inaccurate and is fairly consistent between detectors.

- 
- [1] J. Abadie *et al.*, *Class. Quantum Grav.* **27**, 173001 (2010), arXiv:1003.2480 [astro-ph.HE].
- [2] B. F. Schutz, *Nature* **323**, 310 (1986).
- [3] R. Narayan, B. Paczynski, and T. Piran, *Astrophys. J.* **395**, L83 (1992), astro-ph/9204001.
- [4] D. M. Coward, E. J. Howell, T. Piran, G. Stratta, M. Branchesi, O. Bromberg, B. Gendre, R. R. Burman, and D. Guetta, *Mon. Not. R. Astron. Soc.* **425**, 2668 (2012).
- [5] C. Kim, B. B. P. Perera, and M. A. McLaughlin, *Mon. Not. R. Astron. Soc.* **448**, 928 (2015), arXiv:1308.4676 [astro-ph.SR].
- [6] E. Berger *et al.*, *Astrophys. J.* **664**, 1000 (2007).
- [7] Planck Collaboration, P. A. R. Ade, *et al.*, *ArXiv e-prints* (2015), arXiv:1502.01589.
- [8] J. Abadie *et al.*, *NIMPA* **624**, 223 (2010), arXiv:1007.3973 [gr-qc].
- [9] S. Vitale, W. Del Pozzo, T. G. F. Li, C. V. Van Den Broeck, I. Mandel, B. Aylott, and J. Veitch, *Phys. Rev. D* **85**, 064034 (2012), arXiv:1111.3044 [gr-qc].
- [10] T. B. Littenberg, M. Coughlin, B. Farr, and W. M. Farr, *Phys. Rev. D* **88**, 084044 (2013), arXiv:1307.8195 [astro-ph.IM].
- [11] L. P. Singer *et al.*, *Astrophys. J.* **795**, 105 (2014), arXiv:1404.5623 [astro-ph.HE].
- [12] B. S. Sathyaprakash, B. F. Schutz, and C. van den Broeck, *Class. Quantum Grav.* **27**, 215006 (2010).
- [13] W. Zhao, C. Van Den Broeck, D. Baskaran, and T. G. F. Li, *Phys. Rev. D* **83**, 023005 (2011).
- [14] M. Punturo *et al.*, *Classical and Quantum Gravity* **27**, 084007 (2010).
- [15] S. R. Taylor, J. R. Gair, and I. Mandel, *Phys. Rev. D* **85**, 023535 (2012).
- [16] L. S. Finn, *Phys. Rev. D* **53**, 2878 (1996), gr-qc/9601048.
- [17] S. R. Taylor and J. R. Gair, *Phys. Rev. D* **86**, 023502 (2012), arXiv:1204.6739 [astro-ph.CO].
- [18] C. Messenger and J. Read, *Phys. Rev. Lett.* **108**, 091101 (2012), arXiv:1107.5725 [gr-qc].
- [19] C. Messenger, K. Takami, S. Gossan, L. Rezzolla, and B. S. Sathyaprakash, *Phys. Rev. X* **4**, 041004 (2014), arXiv:1312.1862 [gr-qc].
- [20] D. Eichler, M. Livio, T. Piran, and D. N. Schramm, *Nature* **340**, 126 (1989).
- [21] N. Gehrels *et al.*, *Nature* **437**, 851 (2005), astro-ph/0505630.
- [22] A. J. Castro-Tirado, R. Sanchez-Ramirez, J. Gorosabel, and R. Scarpa, *GRB Coordinates Network* **17278**, 1 (2015).
- [23] B. P. Abbott, R. Abbott, T. D. Abbott, M. R. Abernathy, F. Acernese, K. Ackley, C. Adams, T. Adams, P. Addesso, R. X. Adhikari, and *et al.*, *Living Reviews in Relativity* **19** (2016), 10.1007/lrr-2016-1, arXiv:1304.0670 [gr-qc].
- [24] H.-Y. Chen and D. E. Holz, *Phys. Rev. Lett.* **111**, 181101 (2013).
- [25] L. Z. Kelley, I. Mandel, and E. Ramirez-Ruiz, *Phys. Rev. D* **87**, 123004 (2013), arXiv:1209.3027 [astro-ph.IM].
- [26] K. Siellez, M. Boër, and B. Gendre, *Mon. Not. R. Astron. Soc.* **437**, 649 (2014), arXiv:1310.2106 [astro-ph.HE].
- [27] D. Wanderman and T. Piran, *Mon. Not. R. Astron. Soc.* **448**, 3026 (2015), arXiv:1405.5878 [astro-ph.HE].
- [28] L. Blackburn, M. S. Briggs, J. Camp, N. Christensen, V. Connaughton, P. Jenke, R. A. Remillard, and J. Veitch, *Astrophys. J. Suppl. S.* **217**, 8 (2015), arXiv:1410.0929 [astro-ph.HE].
- [29] S. Fairhurst, *Class. Quantum Grav.* **28**, 105021 (2011), arXiv:1010.6192 [gr-qc].
- [30] J. Abadie *et al.*, *Astrophys. J.* **760**, 12 (2012), arXiv:1205.2216 [astro-ph.HE].
- [31] A. Buonanno, B. R. Iyer, E. Ochsner, Y. Pan, and B. S. Sathyaprakash, *Phys. Rev. D* **80**, 084043 (2009), arXiv:0907.0700 [gr-qc].
- [32] D. A. Brown, I. Harry, A. Lundgren, and A. H. Nitz, *Phys. Rev. D* **86**, 084017 (2012), arXiv:1207.6406 [gr-qc].
- [33] D. Foreman-Mackey, D. W. Hogg, D. Lang, and J. Goodman, *PASP* **125**, 306 (2013), arXiv:1202.3665 [astro-ph.IM].
- [34] W. Fong *et al.*, *Astrophys. J.* **780**, 118 (2014), arXiv:1309.7479 [astro-ph.HE].
- [35] F. Özel, D. Psaltis, R. Narayan, and A. Santos Villalreal, *Astrophys. J.* **757**, 55 (2012), arXiv:1201.1006 [astro-ph.HE].
- [36] J. Abadie *et al.*, *Phys. Rev. D* **85**, 082002 (2012), arXiv:1111.7314 [gr-qc].
- [37] T. Sidery *et al.*, *Phys. Rev. D* **89**, 084060 (2014), arXiv:1312.6013 [astro-ph.IM].
- [38] T. B. Littenberg and N. J. Cornish, *Phys. Rev. D* **91**, 084034 (2015), arXiv:1410.3852 [gr-qc].
- [39] P. Amaro-Seoane *et al.*, *GW Notes* **6**, 4 (2013), arXiv:1201.3621 [astro-ph.CO].
- [40] A. Stroeer and A. Vecchio, *Class. Quantum Grav.* **23**, S809 (2006), astro-ph/0605227.
- [41] W. R. Brown, M. Kilic, J. J. Hermes, C. A. Prieto, S. J. Kenyon, and D. E. Winget, *Astrophys. J. Lett.* **737**, L23 (2011).
- [42] J. J. Hermes *et al.*, *Astrophys. J. Lett.* **757**, L21 (2012), arXiv:1208.5051 [astro-ph.SR].
- [43] M. Kilic, W. R. Brown, and J. J. Hermes, in *9th LISA Symposium*, Astronomical Society of the Pacific Conference Series, Vol. 467, edited by G. Auger, P. Binétruy, and E. Plagnol (2013) p. 47.